Journal of Molecular Catalysis A: Chemical 379 (2013) 294–302

Contents lists available at ScienceDirect

Journal of Molecular Catalysis A: Chemical

journal homepage: www.elsevier.com/locate/molcata

Catalytic consequences of borate complexation and pH on the epimerization of L-arabinose to L-ribose in water catalyzed by Sn-Beta zeolite with borate salts

William R. Gunther, Quynh Duong, Yuriy Román-Leshkov*

Department of Chemical Engineering, Room 66-456, Massachusetts Institute of Technology, Cambridge, MA 02139, USA

ARTICLE INFO

Article history:
Received 7 July 2013
Received in revised form 19 August 2013
Accepted 20 August 2013
Available online 6 September 2013

Keywords:
Sn-Beta zeolite
Borate
Epimerization
Water tolerant solid Lewis acids
Catalytic asymmetric chemistry
Carbohydrate chemistry

ABSTRACT

Sn-Beta zeolite with sodium tetraborate cooperatively catalyzes the epimerization of aldoses via an intramolecular 1,2 carbon-shift mechanism. L-Arabinose is one of the seven common sugars and its epimer, L-ribose, is a valuable rare sugar with applications in antiviral and anticancer agents. Here, a full factorial experimental design is performed to demonstrate the catalytic consequences of varying key reaction parameters such as pH, borate to sugar ratio, and reaction time. Reactivity data revealed that isomerization is favored under acidic pH conditions (pH < 7.0); that epimerization dominates under neutral conditions (pH ranging from 7.0 to 7.8); and that drastic inhibition of both epimerization and isomerization rates occur under basic conditions (pH > 7.8). Using a 5 wt% arabinose feed and 100:1 sugar–metal ratios at 343 K, conversions ranging from 20% to 30% were obtained with selectivities of 75%, 84%, and 91% for boron–sugar ratios of 0.2:1, 0.5:1, and 1:1, respectively. The predominance of epimerization over isomerization products with substoichiometric borate suggests that one borate can influence the reactivity of several sugar molecules and may influence the Sn active site directly. Reaction data obtained under differential conditions revealed that the epimerization reaction follows first order kinetics over a wide temperature range with an apparent activation energy of 98 kJ/mol and pre-exponential factor of 1.9×10^{14} L mol Sn^{-1} s^{-1}.

© 2013 Elsevier B.V. All rights reserved.

1. Introduction

Carbohydrates are involved in important biological processes and also serve as valuable building blocks in many commercial applications. For instance, the common pentose D-ribose is a major component in ribonucleic acid (RNA), adenosine triphosphate (ATP), and nicotinamide adenine dinucleotide (NADH) in metabolism. The industrial production of riboflavin also involves the use of D-ribose [1]. The rare pentose, L-ribose, has found applications in anti-viral and anti-cancer drugs because its reverse stereochemistry alters the interaction with enzymes, inhibiting the nucleoside synthesis-replication process [2]. Additionally, L-RNA binds tightly to natural RNA and is resistant to degradation by nucleases, allowing it to silence gene expression. Consequently, L-ribose is part of several pharmaceuticals presently on the market or undergoing clinical trials [3]. To meet the demand for such rare sugars, costly and complex biochemical [4] and synthetic organic processes are currently used to produce them from common carbohydrates [5]. Therefore, the development of simpler and more effective catalytic pathways to produce rare sugars is of great relevance.

The selective epimerization of aldoses is an attractive pathway for the production of rare sugars. L-Arabinose is a common sugar found in the hemicellulose fraction of biomass. As depicted in Fig. 1, arabinose is interconverted into an equilibrium mixture consisting of ca. 66% arabinose, 11% ribulose and 23% ribose in the presence of isomerase enzymes or inorganic base catalysts at 333 K [6]. Ribulose is the ketose isomer, while ribose is the aldose epimer, typically formed by way of a double isomerization process. The direct epimerization of arabinose into ribose may be accomplished using epimerase enzymes to generate a distribution of 74% arabinose and 26% ribose at 333 K. However, most epimerases only function on substrates modified with phosphate or nucleotide groups. Direct epimerization yields a product distribution that does not contain ribulose, and is therefore more amenable for purification. Epimerization of arabinose to ribose is slightly endothermic, and consequently, high temperatures lead to higher equilibrium ribose yields (see Fig. S1). In this respect, inorganic catalysts may be attractive epimerization candidates given that they are not limited by temperature or substrate functionalization in the same manner as biological catalysts [6].

Hydrophobic zeolites with metal atoms substituted in the crystalline microporous framework have recently emerged as a new

* Corresponding author. Tel.: +1 617 253 7090.
E-mail address: yroman@mit.edu (Y. Román-Leshkov).

1381-1169/$ – see front matter © 2013 Elsevier B.V. All rights reserved.
http://dx.doi.org/10.1016/j.molcata.2013.08.021

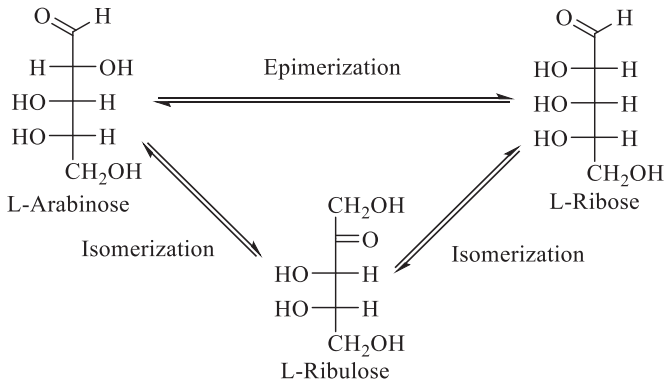

Fig. 1. Schematic representation of the isomerization and epimerization of L-arabinose. The D form is the mirror image of the L form.

class of Lewis acid catalysts capable of activating carbonyl functional groups in the presence of water. The highly dispersed tetrahedrally-coordinated metal centers can accept electron pairs through empty d orbitals and expand their coordination shells from 4 to 5 or 6 sites due to their large covalent radii. Tin-containing zeolites are active in the Meerwein–Ponndorf–Verley reduction [7,8], Baeyer–Villiger oxidation [9–11], and carbonyl-ene reaction [12]. In the context of carbohydrate chemistry, the incorporation of Sn, Ti, and Zr in the framework of Beta zeolite has found applications in the conversion of hexoses [13,14], pentoses [15–18], and trioses [19–22] via intramolecular hydride shifts, as well as in the production of gamma-valerolactone from xylose [23] and alpha-hydroxyacids [24,25] from C-2 and C-4 oxygenates. Recent work shows that Sn-Beta catalyzes the chiral Baeyer–Villiger oxidation of sugar derivatives [26].

Our recent work has shown that Sn-Beta with sodium tetraborate cooperatively catalyzes the selective epimerization of aldoses in aqueous media under mild conditions [27]. The reaction mechanism, investigated using ^{13}C-labeled sugars and nuclear magnetic resonance (NMR), proceeds by way of a 1,2 carbon-shift mechanism whereby C1 forms a new C—C bond with C3, while C2 moves to the C1 position. In the absence of the borate promoter, no carbon backbone rearrangement occurs and Sn-Beta catalyzes a regular aldose–ketose isomerization via an intramolecular hydride shift as reported in previous studies [14]. The epimerization mechanism is analogous to the Bilik reaction using molybdenum-based catalysts that form rigid complexes by interacting with the hydroxyl groups of C1–C4 in the sugar [28,29].

Isomorphic substitution of tin for silicon tetrahedrally-coordinated in the crystalline zeolite framework generates a closed site. Hydration with two water molecules produces a Sn site with octahedral coordination, while hydrolysis of one of the Sn–O–Si bridges generates an open site. For the isomerization of glucose to fructose, Davis and co-workers showed that the open-site in Sn-Beta promotes the ring opening and the hydride transfer steps more favorably than the closed site [30]. In the presence of borate, the 1,2 hydride-shift isomerization pathway is drastically inhibited in favor of a 1,2 carbon-shift epimerization pathway. Interestingly, a similar 1,2 carbon-shift product has been recently reported using Sn-Beta in methanol, although epimerization rates are lower when compared to the Sn-Beta/borate system in water [31]. Borates can interact with the hydroxyl groups found in carbohydrates and with the silanol groups found near the Sn open site, both with a strong dependence on pH [32]. We hypothesize that the borate additive interacts with the sugar and/or the active site to change the reaction from a hydride-shift isomerization to a carbon-shift epimerization pathway. Here, we present a full factorial experimental design to investigate the impact of pH, sugar to borate ratio, and reaction time on the epimerization of L-arabinose to L-ribose. The conversion of arabinose to ribose provided a high value added case to investigate the role of sugar–borate complexation. Understanding which species and reactions are dominant under controlled reaction conditions provides insight into the role of additives in directing the sugar conversion pathway. Thus, we show a comparison of isomerization activity with the fraction of free sugar under low borate loadings and use ^{11}B NMR and Raman spectroscopy characterization to identify sugar borate dimers and polyborates in solution. A temperature study is performed to extract kinetic parameters and optical rotation measurements are used to assess stereospecificity.

2. Experimental

2.1. Catalyst synthesis

Sn-Beta was synthesized as follows: 26.735 g of aqueous tetraethylammonium hydroxide (Sigma–Aldrich, 35% (w/w)) and 24.069 g of tetraethylorthosilicate (Sigma–Aldrich, 99% (w/w)) were added to a Teflon® (Polytetrafluoroethylene, [PTFE]) dish, which was magnetically stirred at room temperature for 90 min and then cooled in an ice bath. Then, 0.261 g of tin (II) chloride dihydrate (Sigma–Aldrich, 98% (w/w)) dissolved in 15 g of cold deionized water (DI H_2O) was added dropwise. Sn(II) which oxidizes to Sn(IV) in water was used in place of $SnCl_4{\cdot}5H_2O$ and has resulted in Sn-Beta consistently free of extraframework SnO_2. The solution was left uncovered on a stir plate for 10 h to reach a total mass of 35 g. Next, 2.600 g of aqueous hydrofluoric acid (Sigma–Aldrich, 48% (w/w)) was added dropwise and the mixture was homogenized using a PTFE spatula, resulting in a thick gel. Then, 0.358 g of previously-made Sn-Beta was seeded into the mixture, which was allowed to evaporate to 33.776 g, which corresponds to a final molar composition of SiO_2/0.01 $SnCl_2$/0.55 TEAOH/0.54 HF/7.52 H_2O. The thick paste was transferred to a 45 ml PTFE-lined stainless steel autoclave and heated to 413 K for 40 days under static conditions. The solids were recovered by filtration, washed with DI H_2O, dried at 373 K and calcined at 853 K for 10 h with a 1 K min^{-1} ramp and 1 h stops at 423 and 623 K, leading to an overall inorganic oxide yield of 80–90%.

Powder X-ray diffraction (PXRD) patterns were collected using a Bruker D8 diffractometer with Cu Kα radiation, which confirmed that the solid material has the Beta topology (see Supplementary Fig. S2). Ultraviolet–visible (UV–vis) measurements were recorded using a Varian Cary 5000 UV–vis-NIR spectrometer with a diffuse reflectance cell after calcination without subsequent drying. The ultraviolet–visible diffuse reflectance spectrum of the calcined sample shows the presence of a unique band at ~200 nm, which has been associated with Sn tetrahedrally coordinated into the zeolite framework (see Supplementary Fig. S3); as additional confirmation of framework incorporation, ^{119}Sn NMR of an analogous sample is included in Fig. S4. Sn content was measured using a Horiba Jobin Yvon ACTIVA-S ICP-AES. Catalyst samples were dissolved in a few drops of 48% HF and diluted in 2% nitric acid after evaporation of the HF.

2.2. Solutions

Within this study, the sugar content was held constant and the borate content was varied to obtain the desired ratios. The sodium to borate ratio was adjusted by mixing boric acid, sodium tetraborate, sodium metaborate and sodium hydroxide on a mass basis on a 50 ml solution scale (see Table S1). The pH was measured with a Mettler Toledo FiveEasy FE20 probe, calibrated with pH 6, 7 and 10 buffers prior to use at 298 K. For the control experiments, the pH-adjusted solutions without borate were very sensitive and were

therefore measured while mixing. NMR solutions were prepared analogously in D_2O on a 5 ml scale.

2.3. Reactions

For the factorial design experiments, Sn-Beta (Si/Sn = 96) was added at a 100:1 sugar–metal molar ratio to a 5 wt% sugar solution in a 5 ml thick-walled glass reactor containing a small magnetic stir bar (typically ~40 mg of catalyst in 2 ml of sugar solution). Reactions were performed with D- and L-arabinose interchangeably with no difference in kinetics. Initial rate experiments were done with larger volumes and higher sugar–metal ratios in order to capture the low conversion data points. In order to determine the initial rates at higher temperature ranges, an arabinose to Sn ratio of 1000 or 2000 was used. The thick-walled glass vials were sealed using a PTFE/silicone septa and metal crimp top, placed in a temperature-controlled oil bath, and removed periodically to take samples. The glass reactors were quenched in ice and a small sample volume was removed. Next, 100 μl of the filtered sample and 25 μl of a 10 wt% mannitol solution were mixed in a vial. The samples were analyzed by high-performance liquid chromatography (HPLC) on an Agilent 1260 system equipped with photodiode array ultraviolet and evaporative light-scattering detectors. The reaction products were separated using a Bio-Rad Aminex HPX-87C column heated to 353 K using deionized water (pH = 7) as the mobile phase at a flow rate of 0.6 ml min^{-1}. Ribulose concentrations were determined using an ultraviolet detector at a wavelength 210 nm. At this wavelength all other sugars had negligible ultraviolet signals. For all ultraviolet-inactive carbohydrates, the analysis was performed using the evaporative light scattering detector. Samples were run in duplicate on the HPLC and the column was regenerated daily with 0.1 M $Ca(NO_3)_2$. Ketoses showed the strongest tendency to shift retention time in the column. Fractionation and NMR were used to check peak purity.

Conversion, selectivity, yield, and turn over frequency (TOF) are defined as follows:

$$\text{Conversion} = \frac{\text{Initial moles of reactant} - \text{Moles of reactant}}{\text{Initial moles of reactant}}$$

$$\text{Selectivity} = \frac{\text{Moles of product} - \text{Initial moles of product}}{\text{Initial moles of reactant} - \text{Moles of reactant}}$$

$$\text{Yield} = \text{Conversion} * \text{Selectivity} = \frac{\text{Moles of product} - \text{Initial moles of product}}{\text{Initial moles of reactant}}$$

$$\text{TOF} = \frac{\text{Moles of converted}}{\text{Moles of Sn} * \text{Time}}$$

2.4. Characterization

Solution NMR was performed on a Varian Inova 500 MHz spectrometer with an Oxford Instruments magnet and 5 mm double-resonance probe, which was tuned to ^1H, ^{11}B, and ^{13}C before use. Samples were prepared at a sugar concentration of 0.05 g ml^{-1} in D_2O using quartz NMR tubes. No correction was made for an isotope effect on the ion product of water. The spinning frequency was 20 Hz. For ^{11}B 128 transients were taken and for ^{13}C 1024 transients were taken. All ^{11}B spectra were referenced using boric acid (H_3BO_3, 19.6 ppm) as a secondary standard relative to boron trifluoride etherate (BF_3 EtO_2). Boric acid was used as an external standard for ^{11}B NMR since the chemical shift for free borate changes with pH. A variable temperature study was also performed in 10 K increments between room temperature and 343 K. ^{13}C NMR was referenced with respect to the C-1 carbon of D-arabinose at 99.47 ppm as a secondary standard relative to 4,4-dimethyl-4-silapentane-1-sulphonic acid.

Raman spectra were acquired on a Kaiser RamanRXN1 spectrometer with a 784.807 nm exciting line from an Invictus diode laser using a HPG-785 grating and a 20× microscope objective. For analysis, a drop of sample was placed on a microscope slide coated with aluminum foil. Post-processing included baseline removal and normalization of the largest peak to an intensity of 1.

Optical rotation measurements were performed with a Jasco P-1010 polarimeter using the 589 nm sodium D line at room temperature. After performing separate epimerizations of L-arabinose and D-arabinose and separation of the products by HPLC, the ribose fraction was dried using a lyophilizer and redissolved in D_2O (see Fig. S5). The optical rotation was measured and used to calculate the specific rotation based on the concentrations determined by HPLC using a power law calibration curve for dilute samples. Solutions were prepared 24 h prior to measurement in order to allow the sugar conformers to equilibrate.

^{119}Sn solid-state MAS NMR experiments were measured using an 8.46-T (^1H, 360.336 MHz) Oxford wide bore magnet and a home-built spectrometer (courtesy of Dr. David Ruben, FBML-MIT). Experiments were performed using a 4-mm Otsuka Electronics MAS double-resonance probe, tuned to ^{119}Sn. Powdered samples were packed into 4 mm outside diameter (o.d.) ZrO_2 rotors equipped with Vespel drive-caps and Kel-F top-caps with O-ring seals. Dry samples were prepared by heating to 473 K under a 0.1 mbar vacuum and loading the NMR rotor in a glovebox. ^{119}Sn spectra were acquired using a Hahn-echo experiment, RD = 1.3*T1, 50 kHz vrf, 2–125 second recycle delays, a spinning frequency of $\omega_r/2\pi$ = 9–10 kHz, and between 70 and 80k co-added transients at 295 K. All ^{119}Sn spectra were referenced with respect to SnO_2 at −604.3 ppm as an external standard relative to trimethyltin. A T1 curve was generated to determine an appropriate relaxation time.

Contour plots were generated by fitting a surface to the experimental data using a linear scattered interpolant, applying five cycles of 40 × 40 point surface convolution using a 3 × 3 matrix with a central weight of 0.4, side weights of 0.1 and corner weights of 0.05, and then stretching this smoothed surface to fit the data using nonlinear parameter fitting. This method avoided data over fitting, the introduction of anomalous peaks due to cubic splines and the use of polynomial surface models which have unusual behavior at the edges of the data. In order to maintain continuity between the sodium to borate and pH plots the pH contour plots were obtained by a conformal mapping of the sodium to borate reactivity surface using a separate pH surface response model. This was possible because reactivity varied smoothly with sodium to borate ratio. Contour lines were determined using a default Origin Delaunay triangulation with B-Spline curves.

3. Results and discussion

Borates have found application in organic synthesis due to their ability to complex with cis-diols of organic molecules [33]. Thus, in the presence of borates, sugars in solution can exist as a free sugar, a one boron one sugar molecular complex (B^-L), a one boron two sugar molecular complex (B^-L_2) and/or a two boron one sugar molecular complex ($B^-)_2L$ (see Fig. S6). The ribose–borate complex is ca. 41 kJ/mol more stable than the arabinose–borate complex [34]. Previous studies have also shown that sugar–borate complexes formed with tetrahedral borate are much stronger than those formed with trigonal borates with complexation timescales considerably faster than those involved in the epimerization reactions [35]. Borates in solution can exist in an uncharged trigonal form, a negatively charged tetrahedral form as well as an intricate

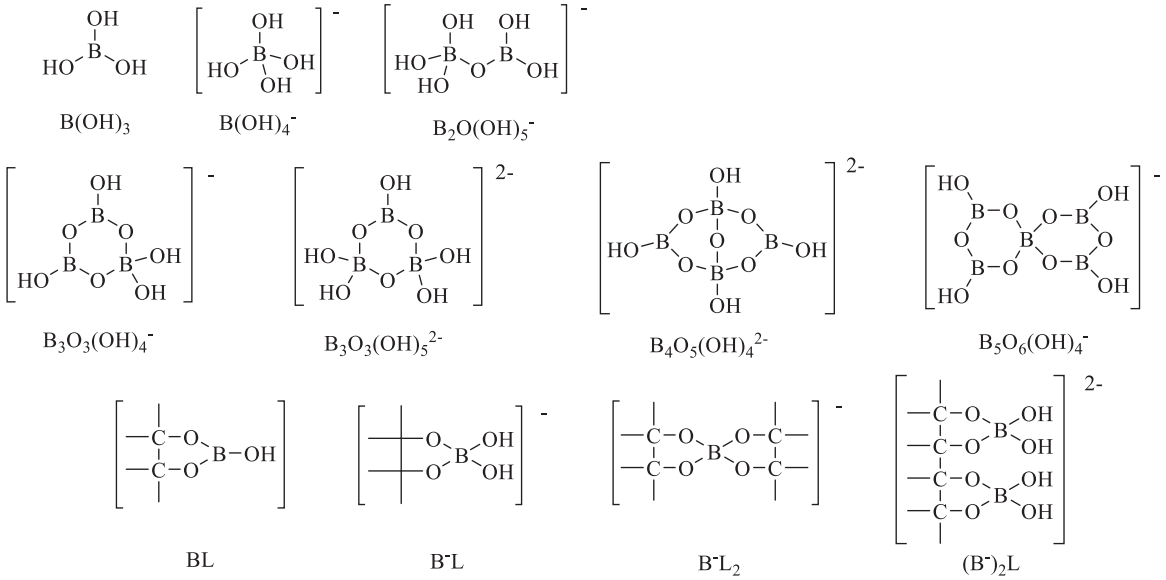

Fig. 2. Schematic representation of borate species in solution and borate–sugar complexes.

polyanionic mixture (see Fig. 2). The nature of the borate speciation in solution is a strong function of pH. For pH < 5 borate exists almost exclusively as boric acid H_3BO_3; for pH > 11 as the tetraborate ion $B(OH)_4^-$; and at intermediate pH values, as a complex mixture of trigonal borate (B), tetrahedral borate (B^-), and borate polyanions [36]. Sodium tetraborate (the borate salt initially used in the Sn-Beta/borate epimerization system) contains two neutral B and two negatively charged B^- species counterbalanced by two sodium cations and, due to charge neutrality arguments, the fraction of tetrahedral boron in solution is equal to the ratio of sodium to boron in the starting material. Thus sodium tetraborate has a B^-/B of 0.5 while, sodium metaborate has a B^-/B of 1. Sodium metaborate corresponds to boric acid fully titrated with sodium hydroxide (NaOH) into tetrahedral borate; therefore, titration of boric acid

Table 1
Full factorial design involving pH, borate to sugar ratio and reaction time as reaction variables for the epimerization of arabinose to ribose.

Entry	Borate–arabinose	B^-/B	pH	BL^-	BL_2^-	15 min			30 min			45 min			60 min		
						C[a] [%]	S1[b] [%]	S2[c] [%]	C[a] [%]	S1[b] [%]	S2[c] [%]	C[a] [%]	S1[b] [%]	S2[c] [%]	C[a] [%]	S1[b] [%]	S2[c] [%]
1	1:1	0.00	3.75	0	0	11	11	24	14	22	27	17	27	26	18	31	26
2		0.23	6.50	0.05	0.12	31	73	5	39	71	4	44	64	5	48	60	5
3		0.41	6.97	0.15	0.26	31	87	3	40	78	2	45	75	2	49	69	4
4		0.50	7.21	0.19	0.31	28	91	3	34	89	4	37	85	4	39	85	5
5		0.64	7.50	0.24	0.38	18	65	1	27	46	1	26	59	1	29	52	1
6		1.00	8.37	0.38	0.46	4	7	2	3	12	5	5	9	2	9	6	1
7	0.5:1	0.00	3.93	0	0	7	5	20	9	17	26	11	22	26	14	25	24
8		0.22	6.51	0.06	0.13	24	64	6	30	61	8	33	55	9	35	49	8
9		0.45	7.02	0.15	0.29	30	82	3	36	77	4	39	76	5	42	69	5
10		0.50	7.11	0.16	0.33	31	84	3	35	81	4	38	80	5	41	75	6
11		0.74	7.49	0.23	0.46	30	65	1	37	60	1	41	60	2	43	58	2
12		1.00	8.37	0.30	0.59	12	52	2	14	56	3	17	47	3	18	49	2
13	0.4:1	0.00	3.98	0	0	10	13	28	13	22	29	15	27	28	19	30	25
14		0.21	6.5	0.05	0.11	22	66	8	27	60	11	30	55	12	32	52	13
15		0.45	6.97	0.15	0.30	31	72	3	37	70	3	41	63	4	45	57	4
16		0.50	7.10	0.16	0.34	29	80	3	33	80	4	37	75	5	39	73	6
17		0.78	7.50	0.24	0.50	27	70	3	33	73	3	37	69	3	40	67	4
18		1.00	7.88	0.30	0.59	14	69	2	16	72	4	19	70	3	18	82	4
19		1.10	8.37	0.31	0.64	9	72	4	12	67	5	16	62	5	17	56	6
20	0.2:1	0.00	4.10	0	0	9	15	29	14	26	30	17	31	27	20	33	24
21		0.21	6.50	0.15	0.29	19	47	11	24	43	13	26	43	15	29	42	15
22		0.46	6.99	0.15	0.29	20	59	3	25	62	4	28	57	5	30	56	6
23		0.50	7.09	0.16	0.33	26	70	4	29	69	6	31	66	7	33	60	8
24		0.80	7.50	0.26	0.48	24	75	2	30	75	4	33	74	4	34	75	4
25		1.00	7.83	0.28	0.59	22	67	3	27	67	4	30	69	5	34	64	5
26		1.10	8.38	0.32	0.64	21	71	4	25	71	5	27.0	75	6	31	64	6
27	0:1	na	4.51	na	na	23	46	23	28	40	29	33	36	31	35	36	35

Reactions were performed at a 100:1 sugar–metal molar ratio with a 5 wt% arabinose feed at 343 K in a stirred batch reactor using Sn-Beta with a Si/Sn of 96. B^-/B fraction is equal to the Na/B ratio used to make the solutions. The fraction BL^- and BL_2^- represent the normalized ^{11}B NMR areas without correction for different NMR transfer efficiencies.

[a] C refers to arabinose conversion.
[b] S1 refers to ribose selectivity.
[c] S2 refers to ribulose selectivity.

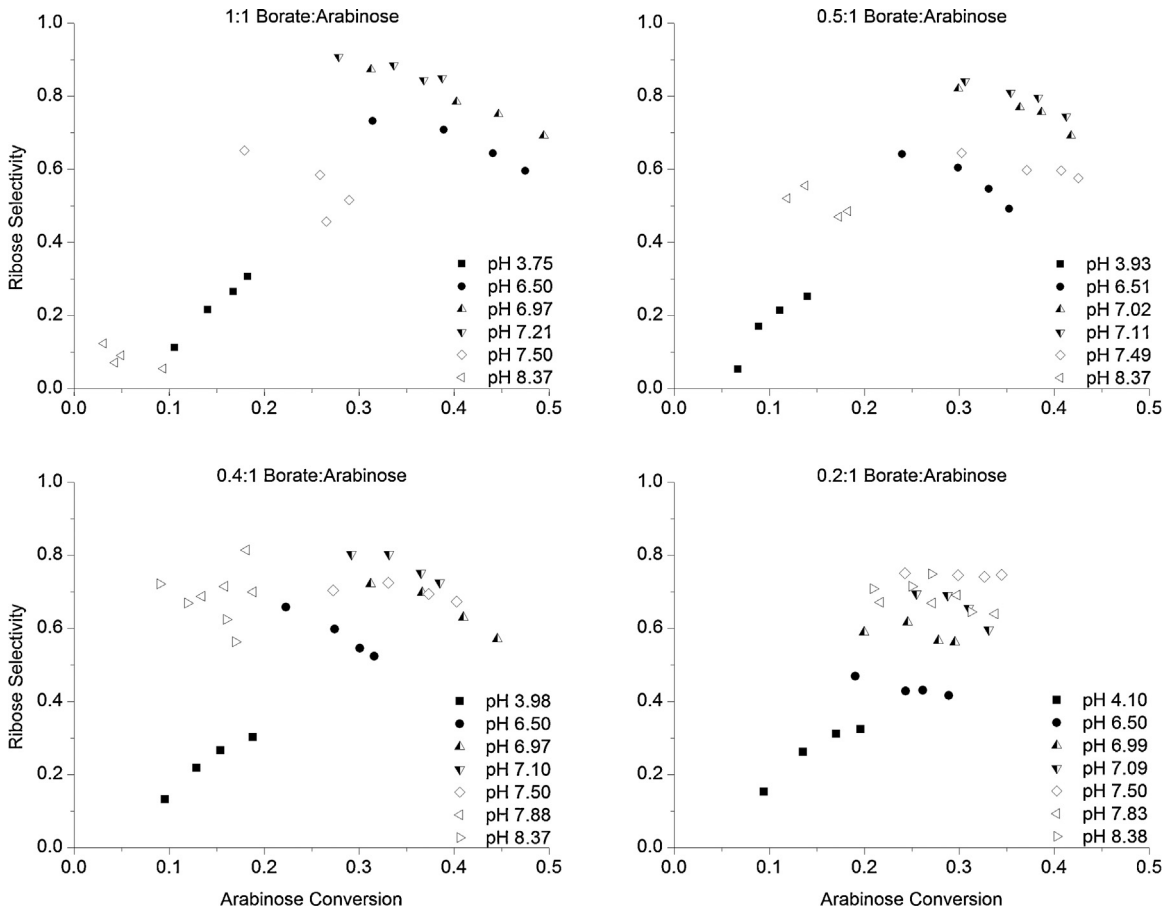

Fig. 3. Factorial design for the conversion of a 5 wt% arabinose solution at 343 K using Sn-Beta and a borate co-catalyst. Reactions were performed at a 100:1 sugar–metal molar ratio with a 5 wt% arabinose feed at 343 K in a stirred batch reactor, using Sn-Beta with a Si/Sn of 96.

with NaOH provides an effective method to control the B^-/B ratio, and, consequently, reaction pH.

Table 1 and Fig. 3 show the results of a full $7 \times 4 \times 4$ factorial design involving pH, sugar to borate ratio, and reaction time as reaction variables for the epimerization of arabinose to ribose. Experiments were designed to facilitate comparison at constant B^-/B and pH. In this manuscript, low pH refers to values lower than 7, near-neutral pH refers to values in the range of 7–7.8, and high pH refers to values of higher than 7.8. In order to relate reactivity to the concentration of borate species, the fraction of B^-L and B^-L_2 was determined with ^{11}B NMR at room temperature (see Supplementary Table S2 and Fig. S10). A separate variable temperature ^{11}B NMR study showed similar spectra up to 343 K with a shift toward monoester at higher temperatures. The ^{11}B data show that the fraction of complexed borate increases steadily with pH and that the ratio between mono and diester is almost constant across the pH spectrum.

The experimental data show that pH has a drastic effect on epimerization selectivity and reactivity. For a solution featuring a 1:1 borate–arabinose ratio, low pH values hindered epimerization pathways, yielding low ribose selectivities <30%. In the presence of the borate additive, a conversion of 11% was obtained at a pH of 3.75 after 15 min at 343 K, whereas in the absence of borates, a conversion of 23% is achieved under similar reaction conditions, thus suggesting that borates slightly inhibit reactivity at low pH values. Conversely, at near-neutral pH conditions ribose selectivities exceeding 50% were obtained, reaching a maximum of 91% at a pH of 7.21. In the pH range of 6.5–7.5, high arabinose conversions ranging from 18% to 32% were observed after 15 min. Note that the observed product distribution contains ribose in excess of the amount predicted from the thermodynamic equilibrium, indicating that the equilibrium is shifted toward the epimer by preferential borate–ribose complexation. At high pH values the reaction rate was drastically inhibited and the low ribose selectivity values obtained (<10%) are not quantitative since the conversion measurements are within the error of the analytical method. When the amount of borate is systematically decreased, the optimal pH to maximize epimerization activity and selectivity gradually increases. For instance, using a 0.2:1 borate–arabinose ratio, a 27% arabinose conversion with 75% selectivity to ribose is obtained at a pH of 8.38 after 45 min. These data also demonstrate that epimerization pathways continue to dominate over isomerization pathways even when substoichiometric amounts of borate are used. The low ribulose yield obtained with substoichiometric borate suggests that borate inhibits isomerization even in the presence of free sugar suggesting that the sugar borate complex is dynamic and could form preferentially in the pores of the zeolite (see Fig. S7). Control experiments and mass balances accounting for >98% of the carbon exclude the possibility of low ribulose yields due to borate–ribulose complexation. These results suggest that one borate molecule may influence the reactivity of many sugar molecules in a catalytic cycle or that borate species remain inside the zeolite pores, potentially influencing the active site directly.

Borate ions are known to catalyze the isomerization of aldoses to ketoses in alkaline media [37]. Control experiments in the presence of borates but in the absence of Sn-Beta were performed to quantify the extent of homogeneous isomerization. Table 2 shows results for reactions performed with 1:1 borate–arabinose solutions. For all

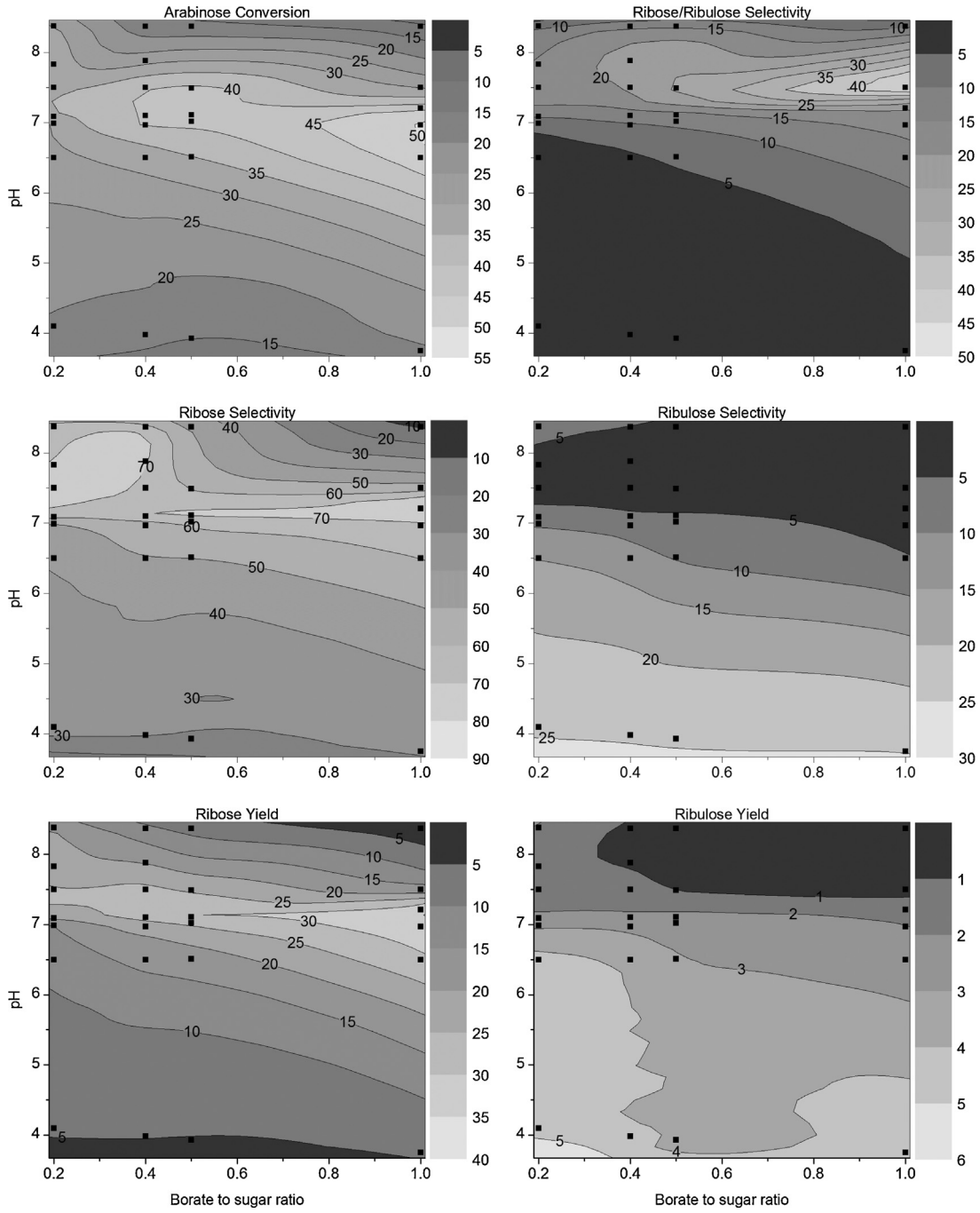

Fig. 4. Contour plots as a function of borate to sugar ratio and pH at 60 minutes for: (a) arabinose conversion, (b) ratio of ribose to ribulose selectivities (i.e., instantaneous selectivity of ribose), (c) ribose selectivity, (d) ribulose selectivity, (e) ribose yield, (f) ribulose yield. The response surface lies the within experimental error of all experimental points which are labeled with dots on the plot. Reactions were performed at a 100:1 sugar–metal molar ratio with a 5 wt% arabinose feed at 343 K in a stirred batch reactor, using Sn-Beta with a Si/Sn of 96.

the pH values investigated, arabinose conversion never exceeded 1% even after 120 min at 343 K. Reactions performed using a combination of Si-Beta and borate were also unreactive.

Fig. 4 shows a series of contour plots mapping the dynamic arabinose conversion and ribose yield as a function of pH ratio and borate–sugar ratio (see Fig. S8 for ribulose study). Note that a near-linear relationship exists between the NaOH–HBO_3 ratio and pH, which is characteristic of weak acid titrations (see Fig. S9). Ribose selectivity and arabinose conversion rates reached their maximum values in near-neutral pH conditions and rapidly tailed off at either extremes of the NaOH–HBO_3 range investigated, thus leading to

Table 2
Control experiments for arabinose conversion in the presence of borates but in the absence of Sn-Beta. Reactions were performed with a 5 wt% arabinose feed at 343 K in a stirred batch reactor.

Arabinose–Borate	B^-/B	pH	Conversion [%]	
			60 min	120 min
1:1	0.00	3.75	<1	<1
	0.23	6.50	<1	<1
	0.41	6.97	<1	<1
	0.64	7.50	<1	<1
	1.00	8.37	<1	<1

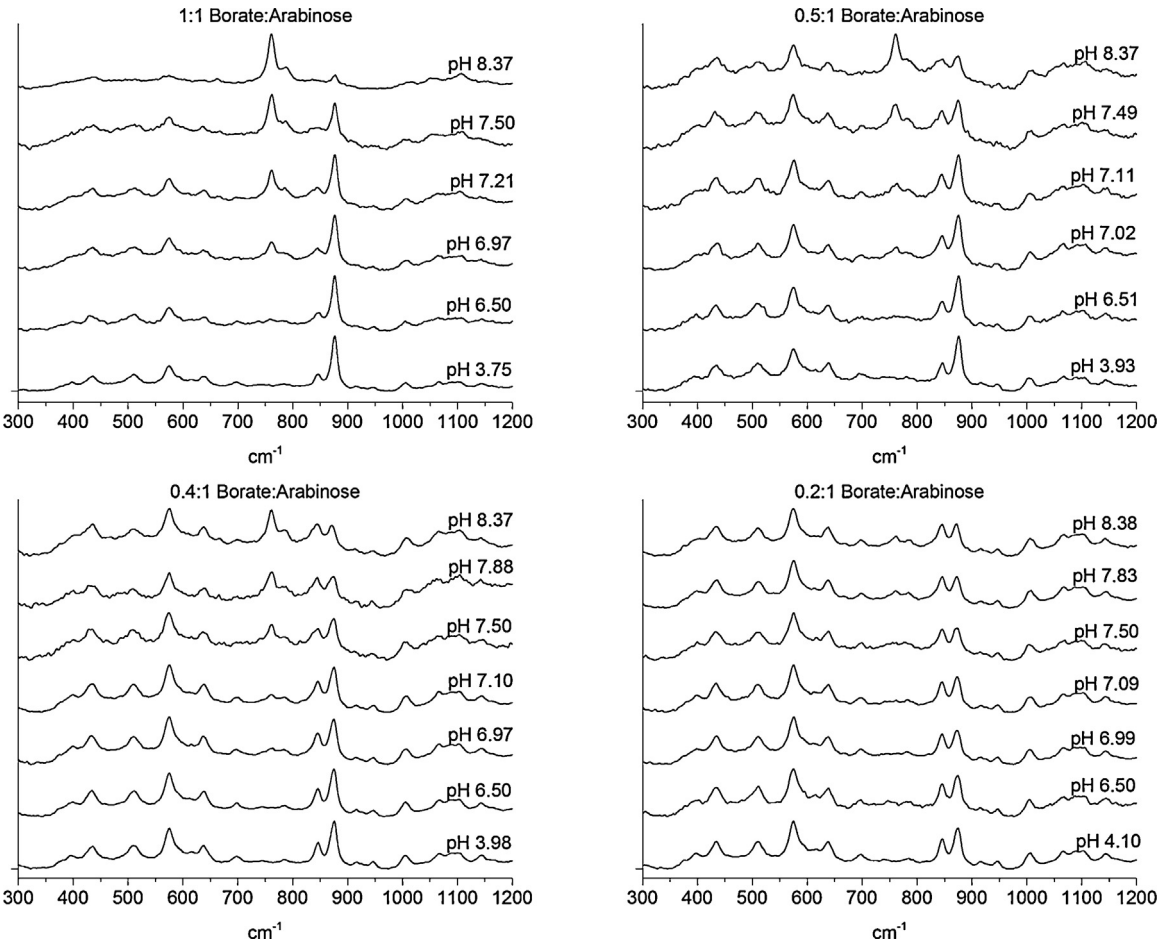

Fig. 5. Raman spectra for 5 wt% arabinose solutions with borate obtained at 298 K.

the appearance of a sharp maximum in ribose yield in the contour plot. In the range where maximum reactivity and selectivity is observed, the ratio of tetragonal to trigonal boron species (i.e. B^-/B) is ca. ~0.5. Diverting from this B^-/B ratio leads to sharp decreases in activity and selectivity, possibly suggesting that both species are required to promote the epimerization pathway. Note that tetragonal borate readily interacts with internal diols in the sugar backbone, whereas trigonal borate can react with hydroxyl groups, such as those present in the Sn open site or in the silanols present next to the Sn open site, via an sp^3d intermediate [32]. The rate constant for arabinose conversion in the presence of borate under acidic conditions is approximately half of that calculated in the absence of borate, thus suggesting that while trigonal borate does not appreciably bind to arabinose it can inhibit the reaction presumably by interacting with the Sn site. Additionally, that the low ribulose selectivity and low unaccounted carbon suggest the isomerization is virtually shut down at neutral pH conditions. Consequently, borate binding may impact the binding of arabinose to the active site and alter elementary steps involved in the hydride shift isomerization mechanism [30]. Studies are currently underway to determine if Sn–O–B are formed during the reaction.

The mechanism for the Bilik reaction involves the formation of a rigid complex between three to four hydroxyl groups of the sugar and a molybdate dimer [38]. Since polyborates occur in near-neutral pH conditions it is plausible that an analogous rigid complex could be formed between a borate dimer and the sugar. Therefore, Raman spectroscopy was used to probe borate-containing solutions at different pH values for the presence of polyborates. As shown in Fig. 5, the resulting spectra clearly show bands at 872 and 745 cm^{-1} corresponding to $B(OH)_3$ and $B(OH)_4^-$ species, respectively; however, no evidence for polyborate species with a sharp maximum at near-neutral pH conditions was found [36]. Resonances corresponding to borate chains were less apparent likely because sugar complexation affects their vibrational frequencies or because they are, in fact, a minor component in the solution. A mechanism that requires polyborates would be difficult to rationalize in the context of steric effects inside the pores of the zeolite and also in view of the carbon-shift epimerization recently observed with Sn-Beta in methanol.

^{11}B NMR was used to further study the complete inhibition of isomerization and epimerization reactions observed under basic conditions (see Fig. S10 and Table S2). At high pH values, the formation of B^-L_2 complexes is slightly favored. We hypothesize that the B^-L_2 complexes formed within the pores may cause pore blocking. Also, the B^-L_2 complexes also lack open B—O—H bonds, effectively decreasing the number of available protons that may participate during key reaction steps, including ring-opening/closing sequences and product desorption from the site [30,39]. Interestingly, Fig. S10 shows a ^{11}B resonance at 10.9 ppm in the BL_2^- region that reaches a maximum as a function of pH for a given borate–arabinose ratio. The pH value at which this maximum is observed increases as the borate–arabinose ratio decreases. A compensation effect is seen wherein the fraction of the BL_2^- species increases in such a way that the ratio of BL_2^- to BL^- remains roughly constant with decreasing borate loadings. Although the presence or absence of B^-L_2 complexes cannot fully explain the inhibition or promotion of reactivity, further studies are required to understand the role of hydroxyl species on reactions rates.

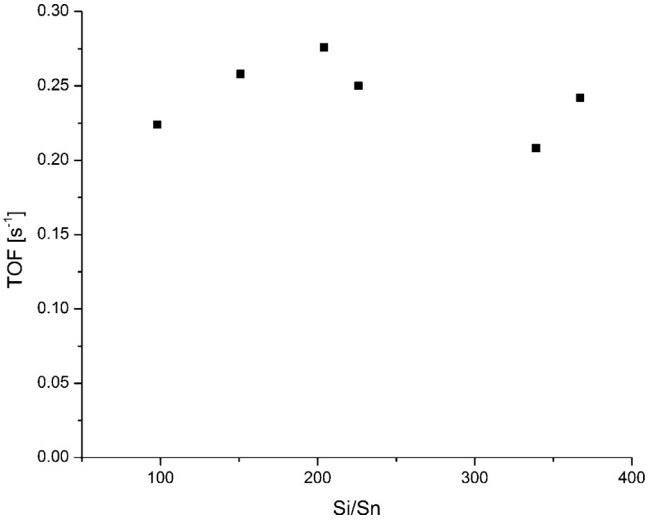

Fig. 6. Madon-Boudart diffusion test at 343 K Experiments were performed with 20 mg of Sn-Beta and a sufficient volume of 5 wt% arabinose to achieve a 2000 sugar–metal ratio in a stirred batch reactor.

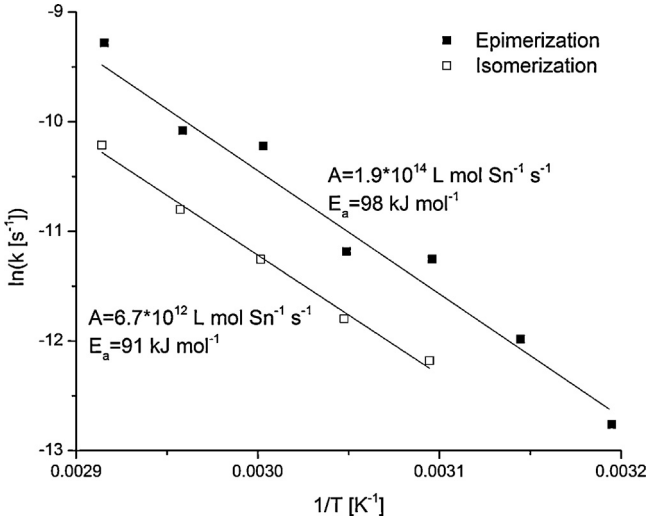

Fig. 8. Arrhenius plot for first order epimerization and isomerization reactions with 1000:1 sugar–metal. Epimerization reactions were performed with a 5 wt% arabinose 1:1 borate–arabinose feed at pH 7.21 in a stirred batch reactor using Sn-Beta with a Si/Sn of 98. Isomerization was performed unbuffered with 5 wt% arabinose.

Kinetic parameters were extracted for arabinose conversion under epimerization conditions. Prior to acquiring reactivity data, an appropriate stirring speed was selected to avoid external intermolecular mass transfer limitations, and a Madon-Boudart test was performed to rule out internal mass transfer limitations. As shown in Figs. 6 and S11, the initial epimerization TOFs remained constant for identical catalyst volumes with zeolites featuring Si/Sn ratios ranging from 98 to 367, thus showing the absence of intra-pore diffusion artifacts at the reaction conditions of interest. Next, the reaction order was determined by varying the feed concentration under differential conditions over a wide range of concentrations (see Figs. 7 and S12). Turnover rates were determined by normalizing the moles of arabinose converted by the total moles of Sn on each catalyst at conversion levels <15%. As shown in Fig. 7, arabinose epimerization follows first order kinetics, thus suggesting that sugar coverage at the active site is low under the reaction conditions investigated. An Arrhenius plot was used to calculate an apparent activation energy of 98 kJ/mol and pre-exponential factor of 1.9×10^{14} L mol Sn^{-1} s^{-1} for the epimerization reaction (see Fig. 8, Table S3 and Fig. S13). Ribose selectivity remained high for all temperatures investigated, indicating that homogeneous side reactions were not dominant. The amount of ribose formed from ribulose isomerization (i.e., 1,2 hydride-shift pathway) with respect to that formed from arabinose epimerization (i.e., 1,2 carbon-shift pathway) was estimated from ^{13}C NMR data of reaction products obtained using [^{13}C1]arabinose feeds. A 5:1 arabinose–borate solution reacted at pH 7.21 for 60 min yielded ca. 29% [^{13}C2]ribose C1, 4% [^{13}C1]ribose, and 2% [^{13}C1]ribulose. The ratio of [^{13}C1]ribose to [^{13}C1]ribulose is approximately equal to the isomerization thermodynamic equilibrium value (see Figs. S14 and S15). The NMR data for reactions performed with stoichiometric borate show that a similar product distribution is obtained to that of the 5:1 arabinose:borate case. Further, initial rate data show that the [^{13}C2]ribose and the [^{13}C1]ribulose selectivity remains constant at low conversions, which is consistent with a reaction pathway that does not involve ribulose as an intermediate (see Table S4). These data suggest that the observed arabinose consumption corresponds predominantly to ribose production via the 1,2 carbon-shift epimerization pathway.

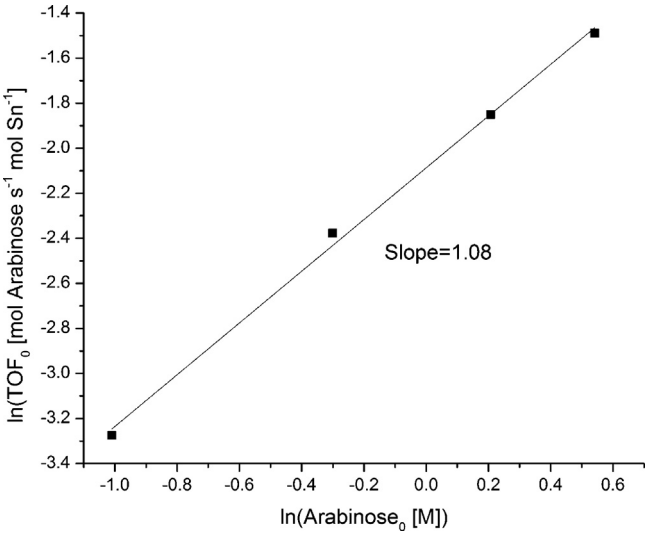

Fig. 7. Reaction order plot for initial rates at 343 K and 1000:1 sugar–metal with a 5 wt% arabinose 1:1 borate–arabinose solution at pH 7.21 in a stirred batch reactor. The catalyst used was Sn-Beta with a Si/Sn of 98.

Analogous kinetic experiments were performed in the absence of borate. An apparent activation energy of 91 kJ/mol and a pre-exponential factor of 6.7×10^{12} L mol Sn^{-1} s^{-1} were obtained for arabinose isomerization (see Supplementary Table S3 and Fig. S16). These values are similar to the energy barriers previously calculated for glucose [30]. Thus, under optimal conditions, the epimerization rate constant at 343 K (0.23 L mol Sn^{-1} s^{-1}) is roughly twice that of the isomerization without borate (0.093 L mol Sn^{-1} s^{-1}) and the similarities between the isomerization and epimerization kinetics are consistent with a common intermediate such as the open chain form of the sugar. The differences in rates are mostly associated with differences in the pre-exponential factors. The higher pre-exponential factor observed for the epimerization of borates may result from more favorable open vs. closed site distribution in the presence of borate or due to a dual Lewis acid activation wherein borate contributes to spatially arrange the sugar in a more desirable configuration near the active site.

Optical rotation measurements demonstrated the stereospecific nature of the epimerization reaction. The specific rotation of a sugar varies with solvent and borate concentration, and requires time to equilibrate, making it difficult to determine an enantiomeric excess [40]. Optical rotation results shown in Table 3, confirm the

Table 3
Optical rotation measurement used to assess stereospecificity.

Carbohydrate[a]	$[\alpha]_D$
Literature D-ribose[41]	−18.8 to −23.7
Literature L-ribose[41]	18.7–24.0
Ribose from D-Arabinose	−14
Ribose from L-Arabinose	21

[a] Literature values are at 274 K while experimental values are at 298 K.

stereospecific nature of the epimerization reaction using Sn-Beta in conjunction with borate salts.

4. Conclusion

A full $7 \times 4 \times 4$ factorial experimental design for NaOH–HBO_3 (i.e., pH), sugar to borate ratio, and reaction time facilitated optimization of ribose production and showed that low pH values favored isomerization pathways, near-neutral pH values favored epimerization pathways and high pH values inhibited both epimerization and isomerization. Optimal pH values ranging from 7.0 to 7.5 and high borate to sugar ratios were found to promote borate complexation with the sugar, effectively decreasing the concentration of free arabinose and promoting epimerization via a 1,2 carbon-shift mechanism. Importantly, 1,2 carbon-shift epimerization products dominated most product distributions even when using substoichiometric amounts of borate, thus suggesting a potential interaction of borate species with the active site that inhibits isomerization pathways. Reactivity and ^{11}B NMR characterization data showed that although the fraction of complexed sugar (B^-L and B^-L_2) increases with pH, reactivity declines at high pH values, thus indicating that the fraction of complexed borate is not a sufficient descriptor of reactivity. The maximum in reactivity as a function of pH is consistent with both charged and uncharged borates partitioning into the zeolite and participating in the reaction. The Sn-Beta/borate system shows high epimerization activity at low temperature following a first order rate law over a wide temperature range. Optical rotation measurements confirmed the stereospecific nature of the epimerization reaction. The isolated Lewis acid sites inside the hydrophobic zeolite present an interesting opportunity to study the Sn-borate catalytic pair and the unusual C—C bond-forming and bond-breaking events it promotes. Future studies are geared at understanding the nature of the borate interaction with the active site.

Appendix A. Supplementary data

Supplementary data associated with this article can be found, in the online version, at http://dx.doi.org/10.1016/j.molcata.2013.08.021.

References

[1] R. Wolf, F. Reiff, R. Wittmann, J. Butzke, Process for the preparation of riboflavin, U.S. Patent US4355158 A, 1982.
[2] K. Okano, Tetrahedron 65 (2009) 1937–1949.
[3] N. Wymer, P. Taylor, Production of L-ribose and other rare sugars, US Patent App. 11/501,997, 2006.
[4] C. Hu, L. Li, Y. Zheng, L. Rui, Appl. Microbiol. Biotechnol. 92 (2011) 449–455.
[5] M. Akagi, D. Omae, Y. Tamura, Chem. Pharm. Bull. 50 (2002) 866–868.
[6] Y. Tewari, R. Goldberg, Biophys. Chem. 22 (1985) 197–204.
[7] A. Corma, M.E. Domine, S. Valencia, J. Catal. 215 (2003) 294–304.
[8] A. Corma, M.E. Domine, L. Nemeth, S. Valencia, J. Am. Chem. Soc. 124 (2002) 3194–3195.
[9] A. Corma, L.T. Nemeth, M. Renz, S. Valencia, Nature 412 (2001) 423–425.
[10] A. Corma, M.T. Navarro, M. Renz, J. Catal. 219 (2003) 242–246.
[11] H.Y. Luo, L. Bui, W.R. Gunther, E. Min, Y. Román-Leshkov, ACS Catal. 2 (2012) 2695–2699.
[12] A. Corma, M. Renz, Arkivoc 2007 (2007) 40–48.
[13] Y. Román-Leshkov, M. Moliner, J.A. Labinger, M.E. Davis, Angew. Chem. Int. Ed. 49 (2010) 8954–8957.
[14] M. Moliner, Y. Román-Leshkov, M.E. Davis, PNAS 107 (2010) 6164–6168.
[15] M.S. Holm, Y.J. Pagán-Torres, S. Saravanamurugan, A. Riisager, J.a. Dumesic, E. Taarning, Green Chem. 14 (2012) 702.
[16] C.M. Lew, N. Rajabbeigi, M. Tsapatsis, Microporous Mesoporous Mater. 153 (2012) 55–58.
[17] V. Choudhary, A.B. Pinar, S.I. Sandler, D.G. Vlachos, R.F. Lobo, ACS Catal. 1 (2011) 1724–1728.
[18] V. Choudhary, S.I. Sandler, D.G. Vlachos, ACS Catal. 2 (2012) 2022–2028.
[19] M.S. Holm, S. Saravanamurugan, E. Taarning, Science 328 (2010) 602–605.
[20] F. de Clippel, M. Dusselier, R. Van Rompaey, P. Vanelderen, J. Dijkmans, E. Makshina, et al., J. Am. Chem. Soc. 134 (2012) 10089–10101.
[21] L. Li, C. Stroobants, K. Lin, P.A. Jacobs, B.F. Sels, P.P. Pescarmona, Green Chem. 13 (2011) 1175–1181.
[22] P.P. Pescarmona, K.P.F. Janssen, C. Delaet, C. Stroobants, K. Houthoofd, A. Philippaerts, et al., Green Chem. 12 (2010) 1083–1089.
[23] L. Bui, H. Luo, W.R. Gunther, Y. Román-Leshkov, Angew. Chem. Int. Ed. 52 (2013) 8022–8025.
[24] M. Dusselier, P. Van Wouwe, S. De Smet, R. De Clercq, L. Verbelen, P. Van Puyvelde, et al., ACS Catal. 3 (2013) 1786–1800.
[25] M. Dusselier, P. Van| Wouwe, F. de| Clippel, J. Dijkmans, D.W. Gammon, B.F. Sels, ChemCatChem 5 (2013) 569–575.
[26] C. Paris, M. Moliner, A. Corma, Green Chem. 15 (2013) 2101.
[27] W.R. Gunther, Y. Wang, Y. Ji, V.K. Michaelis, S.T. Hunt, R.G. Griffin, Y. Román-Leshkov, Nat. Commun. 3 (2012) 1109.
[28] L. Petruš, M. Petrušová, Z. Hricovíniová, Glycoscience 215 (2001).
[29] A. Köckritz, M. Kant, M. Walter, A. Martin, Appl. Catal., A 334 (2008) 112–118.
[30] R. Bermejo-Deval, R.S. Assary, E. Nikolla, M. Moliner, Y. Román-Leshkov, S.-J. Hwang, et al., Proc. Natl. Acad. Sci. U. S. A. 109 (2012) 9727–9732.
[31] R. Bermejo-Deval, R. Gounder, M.E. Davis, ACS Catal. 2 (2012) 2705–2713.
[32] A. Irwin, J. Holmgren, T. Zerda, J. Jonas, J. Non-Cryst. Solids 89 (1987) 191–205.
[33] C.J. Cowden, I. Paterson (Eds.), Organic Reactions, John Wiley & Sons, Inc., Hoboken, NJ, 2004.
[34] J.E. Sponer, B.G. Sumpter, J. Leszczynski, J. Sponer, M. Fuentes-Cabrera, Chemistry 14 (2008) 9990–9998.
[35] R. van den Berg, J.a Peters, H. van Bekkum, Carbohydr. Res. 253 (1994) 1–12.
[36] T. Hirao, M. Kotaka, H. Kakihana, J. Inorg. Nucl. Chem. 41 (1979) 1217–1220.
[37] J. Mendicino, J. Am. Chem. Soc. 402 (1960) 4975–4979.
[38] L. Petruš, M. Petrušová, Z. Hricovíniová, in: A. Stütz (Ed.), Topics in Current Chemistry, Springer Berlin, Heidelberg, 2001, pp. 15–41.
[39] R.S. Assary, L.A. Curtiss, J. Phys. Chem. A 115 (2011) 8754–8760.
[40] D. Adam, R.P. Jennings, Proc. South African Sugar Technol. Assoc., 1966, pp. 206–213.
[41] F. Phelps, H. Isbell, W. Pigman, J. Am. Chem. Soc. 3226 (1934) 747–748.